AIAA 90-1399
Shock-Tube Calibration of a Fast-Response Pressure Transducer

K. Chung and F. Lu
Univ. of Texas
Arlington, TX

AIAA 16th Aerodynamic Ground Testing Conference

June 18-20, 1990 / Seattle, WA

Shock-Tube Calibration of a Fast-Response Pressure Transducer

Kung-Ming Chung* and Frank K. Lu†
The University of Texas at Arlington, Arlington, Texas

The sensitivity of a miniature fast-response piezoresistive pressure transducer determined dynamically was found to be slightly higher than that determined statically. Thus, mean pressures in a turbulent or unsteady flowfield that are measured using statically-calibrated pressure transducers would be slightly above true values. Unsteady pressure measurements to obtain space-time correlations and spectra can, however, be properly performed if the slight error is acceptable. These measurements are, obviously, subjected to limitations imposed by the bandwidth and the spatial resolution of the transducer. The noise spectrum revealed that the noise is predominantly above the transducer's resonant frequency. Filtering to improve the signal-to-noise ratio is particularly necessary when using the transducers at their low range. Transducer drift increases the signal-to-noise ratio and can adversely affect mean measurements.

Nomenclature

a	= speed of sound, $\mathrm{m\,s^{-1}}$ (ft/sec)
A/D	= analog-to-digital
c	= transducer sensitivity, μV/Pa (mV/psia)
g	$= \left\{\left[\frac{2+(\gamma_4-1)M_{3a}^2}{2+(\gamma_4-1)M_{3b}^2}\right]^{1/2} \times \left[\frac{2+(\gamma_4-1)M_{3b}}{2+(\gamma_4-1)M_{3a}}\right]\right\}^{2\gamma_4/(\gamma_4-1)}$
ID	= internal diameter
M	= Mach number
p	= pressure, Pa (psi)
S/N	= signal-to-noise
T	= temperature, K (°F)
U	= speed, $\mathrm{m\,s^{-1}}$ (ft/sec)
V	= transducer output, mV
Δl	= transducer spacing, mm (in)
γ	= specific-heat ratio
σ	= standard deviation

Superscripts

$'$	= fluctuating
$(\bar{})$	= mean

Subscripts

s	= shock
1, 2, 3, 3a, 3b, 4, 5	= regions defined in Fig. 1b

Introduction

Experimental studies of rapidly changing pressures have relied on miniature fast-response pressure transducers. Examples of the use of such transducers abound in acoustics, turbulence, and shock-wave and blast-wave research. Recently, there has been an upsurge of interest in the study of compressible turbulent boundary layers, particularly shock boundary-layer interactions, through surface pressure measurements [1]. These measurements using fast-response transducers seek to understand the unsteady aspects of the interaction such as shock oscillations.

Also, miniature fast-response pressure transducers are by necessity used in impulse facilities. In the past, the signals were recorded by analog devices such as oscilloscopes and magnetic tape recorders or by low-resolution (8-bit) A/D converters. Precise determination of transducer characteristics was not necessary or even possible with these antiquated recording devices.

However, accurate measurements made possible by advances in data acquisition require that fast-response transducers be better understood than in the past. Such understanding will allow these transducers' advantages and limitations to be appreciated. One difficulty faced by many investigators is the question of whether static calibrations can be used instead of dynamic calibrations. Obviously, a static calibration can be performed with relative ease. Further, previous investigators [2, 3, 4] relied on Raman's [5] work which showed that dynamic calibration values of mean pressure are systematically about 5% lower than those obtained from static calibrations. The motivation of the present study is, therefore, to re-examine this difference by performing static and dynamic calibration using more modern equipment. In addition, the noise and drift characteristics of such transducers were also

*Graduate Research Assistant, Aerospace Engineering Department. Student Member AIAA.

†Assistant Professor, Aerospace Engineering Department. Member AIAA.

examined.

There are many ways of dynamically calibrating pressure transducers [6, 7, 8]. In principle, a known and rapidly changing pressure is applied to the transducer whose output is measured precisely to obtain the transducer's transfer function [9]. Different inputs can be used in this determination. One possibility is to impose a step change which, in practice, can be obtained by a propagating shock wave in a shock tube. Unlike quick-opening or explosive devices, the shock tube produces a very steep pressure rise whose magnitude can be precisely controlled. The present calibration, hence, used a shock tube.

Experimental Methods

The Shock Tube

The pilot shock tube, located at the Aerodynamic Research Center (ARC) of The University of Texas at Arlington, consisted of a 2.1-m (7-ft) long, 100-mm (4-in) ID driver tube connected to a 6.1-m (20-ft) long, 50-mm (2-in) ID driven tube via a double-diaphragm section, Fig. 1a. At the end of the driven tube was mounted a 0.3-m (1-ft) long, 50-mm (2-in) ID test section whose downstream end was bolted to a dump tank. The driven tube was long enough to allow the propagating shock to develop fully. In the present experiments, only a single, unscored mylar diaphragm, 0.5 mm (0.023 in) thick, was used to separate the driver and driven gases. Both gases were air.

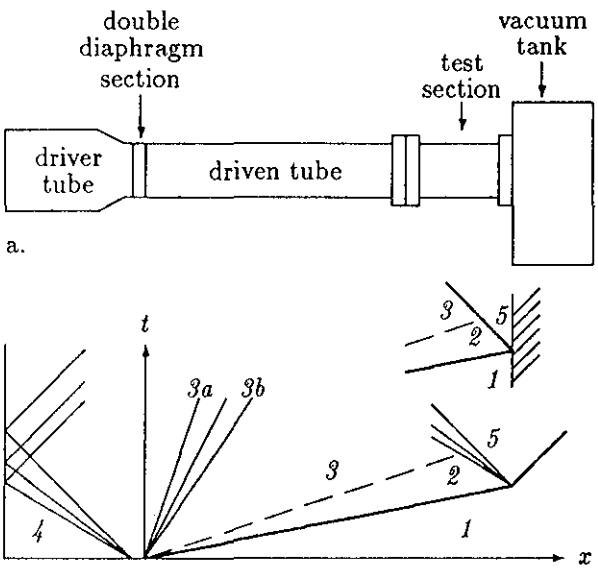

Figure 1: Pilot shock tube. a. Schematic of facility. b. Wave diagram of flow with vacuum tank attached to shock tube.

Air from the ARC's 14 MPa (2,000 psia) air supply and storage system was regulated to about $p_4 = 2.0 \pm 0.07$ MPa (285 ± 10 psia) for all test runs, p_4 being measured by a Wika gauge with a ± 70 kPa (± 10 psia) accuracy. Although an accurate measurement of p_4 may appear necessary at first, this is not really so. The step pressure rise to p_2 was more accurately determined from the shock Mach number

$$M_s = U_s/a_1 \tag{1}$$

and initial conditions in the driven tube (*1* in Fig. 1b), namely [10]:

$$p_2 = p_1 \left[1 + \frac{2\gamma_1}{\gamma_1 + 1}\left(M_s^2 - 1\right)\right]. \tag{2}$$

The driven tube was evacuated by a Sargent-Welch Model 1396 vacuum pump to a range of p_1 from 0.4 to 7 kPa (0.06–1 psia). The vacuum was measured accurately to ± 7 Pa (± 0.001 psia) by an MKS Baratron Model 127A vacuum gauge, a capacitance-type manometer widely used as a secondary standard [11].

The transducer being calibrated was mounted 76 mm (3 in) from the test-section leading edge. Inline with this transducer and $\Delta l = 100$ mm (4 in) downstream was mounted another similar transducer. These two transducers were used to time the shock passage from which M_s could be evaluated. The transducers were flushmounted as best as possible, minimizing the protrusion of the flat transducer face above the curved inner surface of the test section.

When the diaphragm was ruptured, a wave system was set up. This system is illustrated in an x-t diagram in Fig. 1b where the regions of interest are labeled conventionally. The wave diagram is drawn assuming one-dimensional, inviscid, perfect gas flow. Fig. 1b illustrates the case where p_4/p_1 is sufficiently large to choke the converging portion of the diaphragm section, resulting in an unsteady supersonic expansion in *3*. Otherwise, subsonic flow exists in this region. The inset to Fig. 1b illustrates the wave pattern if the end of the test section was closed.

Shock Tube Principles

For an unheated driver gas, it is usual to express the diaphragm pressure ratio p_4/p_1, the driver-to-driven tube area ratios A_4/A_1 and the Mach in region *3* M_3 as follows [12]:

$$\frac{p_4}{p_1} = \frac{p_2}{p_1} g^{-1} \left[1 + \frac{\gamma_4 - 1}{2} M_3\right]^{2\gamma_4/(\gamma_4 - 1)} \tag{3}$$

$$\frac{A_4}{A_1} = \frac{M_{3b}}{M_{3a}} \left[\frac{2 + (\gamma_4 - 1) M_{3a}^2}{2 + (\gamma_4 - 1) M_{3b}^2}\right]^{(\gamma_4 - 1)/[2(\gamma_4 - 1)]} \tag{4}$$

$$M_3 = \left[\frac{a_1}{U_2}\frac{a_4}{a_1} g^{[(\gamma_4 - 1)/2\gamma_4]} - \frac{\gamma_4 - 1}{2}\right]^{-1}. \tag{5}$$

To solve for the four unknowns, M_s, M_3, M_{3a} and M_{3b}, using the above equations, a boundary condition must

be imposed, namely that $M_3 = M_{3b}$ if $M_3 < 1$ or $M_{3b} = 1$ if $M_3 \geq 1$. With air in the driver and driven tubes, results from computations using the above equations are plotted in Fig. 2. Also plotted in the figure are some of the present results which will be discussed later. The theory predicts that

$$\lim_{p_4/p_1 \to \infty} M_s \to 6.4 \quad \text{and} \quad \lim_{p_4/p_1 \to \infty} p_2/p_1 \to 51.2. \tag{6}$$

In practice, the shock tube cannot operate with extremely large diaphragm pressure ratios and M_s tends to be limited to about 3 at most (for air) as is also the case in the present experiments. (But by using a light driver gas such as helium or by heating the driver gas, M_s can be increased without unduly large initial pressure ratios.)

The inviscid computations enabled the initial pressures, p_1 and p_4, to be selected such that a sufficient range of M_s and, therefore, p_2 was obtained while at the same time ensuring that the transducer did not suffer damage from overpressurization. In the case of the close-ended test section (wave diagram shown as inset to Fig. 1b), it can be seen that $p_5 > p_2 > p_1$. For the values of p_1 and p_4 attainable in the pilot shock tube, the transducer could not be mounted at the end of a closed tube for three reasons. The first is that the (pitot) pressure sensed by the transducer would, in most instances, be larger than the transducer's overpressure rating (140 kPa, 20 psia). The second is that p_5 will also be mostly too large. Thirdly, with a close-ended tube, the final pressure level of the entire shock tube may rise beyond the overpressure rating of the transducer. Thus, the transducer was calibrated by mounting it to the test-section wall, with a large dump tank attached to the test section to ensure that the final pressure level at the end of a run was below atmospheric.

The shock Mach number must also be carefully chosen. Too small a value of M_s, in which there is no unsteady expansion in $\mathcal{I}$, may cause p_2 to be too large. Too large a value of M_s, on the other hand, can produce excessively high pressures, p_{3a}, behind the unsteady expansion.

The time required for shock passage across the two transducers, Δt, can be resolved to 2 μs, the sampling interval of the data acquisition system. Thus,

$$U_s = \Delta l / \Delta t, \tag{7}$$

from which M_s can be evaluated using Eqn. (1) to $\pm 1\%$. This local value of M_s enabled a more representative evaluation of the flow properties across the shock propagating past the transducer than if the shock Mach number was obtained from timing the shock passage through the driven tube. This is because the shock formation and propagation are strongly affected by the diaphragm bursting process and by the boundary-layer growth behind the shock. Both factors reduce M_s as can be seen in the present experimental data displayed in Fig. 2. (In addition, the available test time was also reduced below inviscid predictions due to contact surface diffusion.)

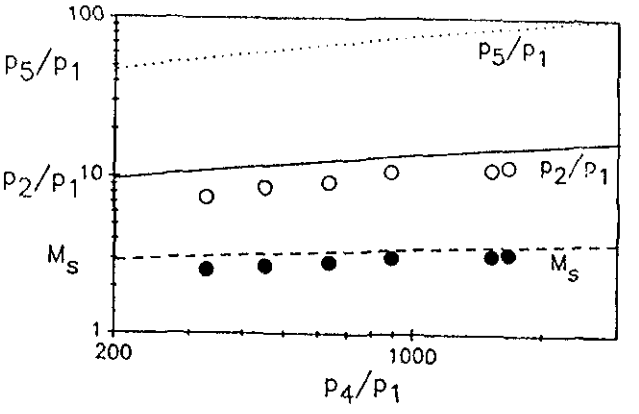

Figure 2: Shock Mach number, shock strength and reflected shock strength as a function of initial pressure ratio (air in driver and driven tubes).

The Pressure Transducer

The transducer that was calibrated was a Kulite XTS-190-10A with a 0–70 kPa (0–10 psia) range. Kulite transducers are of solid-state integrated-circuit design and are widely used in fluids measurements because of their ruggedness, miniature size, sensitivity, high-frequency response and wide dynamic range. The sensor consists of a silicon diaphragm on which four piezoresistive strain gauges form a Wheatstone bridge. For a discussion of the transduction principles, see Refs. [6, 7].

Some pertinent characteristics quoted in the manufacturer's specifications are a resonant frequency of 70 kHz, fullscale output of 100 mV and a combined nonlinearity and hysteresis of $\pm 0.3\%$ fullscale. For the particular transducer under test, the manufacturer's calibration gave a sensitivity of 1.22 μV/Pa (8.38 mV/psia).

In the present experiments, the transducer was excited by a Hewlett-Packard Model 6235A power supply set to 10.000 ± 0.001 VDC (checked throughout the test program by a $5\frac{1}{2}$-digit Hewlett-Packard Model 3468A digital multimeter.) This excitation voltage was the same as that used in the manufacturer's static calibration.

Signal Conditioning, Data Acquisition & Data Processing

The signals from the pressure transducers were lowpass filtered at 60 kHz by a Krohn-Hite Model 3202R filter and then digitized at 500 kilosamples/s by a LeCroy data-acquisition system [13, 14] (Fig. 3). This sampling rate far exceeded the minimum necessary to prevent aliasing of the digitized signal. Each record consisted of 4 096 datapoints. The LeCroy system was operated to capture pre-trigger data, the trigger being activated by a sufficiently high pressure level upon passage of the expansion (*3a–3b* in Fig. 1b) over the front transducer.

The programmable amplifiers in the LeCroy Model 6810 waveform digitizer were set to the 0–400 mV range. Thus the 12-bit A/D conversion implied a digitizing accuracy of just under 0.1 mV/bit. Without further preamplification, this resulted in a percentage accuracy of 0.15–6.1% in the A/D conversion for the pressure ranges encountered.

The digitized signals were transmitted via a pair of National Instruments Model GPIB-100 bus extenders to an Everex Step 286 microcomputer and stored for analysis. Control of the data-acquisition system was by LeCroy CATALYST software while data reduction was performed using ASYSTANT software.

Experimental Procedure

Noise & Drift Measurements

In a subsidiary set of experiments, atmospheric pressure data (100.3 kPa, 14.55 psia) were recorded at three temperatures: 0 °C (32 °F), 21 °C (70 °F) and 100 °C (212 °F). The cold and hot measurements were done using an ice bath and a boiling-water bath respectively, with the transducer protected in a test tube. Data were recorded after 30 minutes of immersion to ensure that the transducer's temperature had equilibrated. In addition, in the static calibrations (see below), extra data were recorded at vacuum pressures but at 21 °C only. In all of these measurements, to capture the noise, the data were not filtered. To determine drift at 21 °C and at different mean pressures during static calibrations, the unfiltered transducer output was sampled at one kilosamples/s which gave a spectrum up to 500 Hz. The sampling period was 8 s and 8 192 datapoints were obtained.

Static & Dynamic Calibrations

Static calibration was performed by recording the filtered transducer output and the Baratron vacuum gauge reading at several steps during evacuation of the driven tube. The driven tube pressure was held steady during data acquisition. Static calibrations were repeated daily throughout the test program. Further, at some points of the evacuation, noise and drift data from unfiltered signals were also taken as described. Anticipating the results, the transducer calibration was found to follow

$$p = V/c, \tag{8}$$

where c is the sensitivity of the transducer.

For dynamic calibration, the driver tube was first pressurized to about 0.7 MPa (100 psia), which was less than the 2 ± 0.07 MPa (275 ± 10 psia) pressure which would cause diaphragm rupture. Simultaneously, the driven tube was evacuated to the desired p_1 value. Further pressurization of the driver tube to about 2 MPa then ruptured the diaphragm. As previously stated, precise control of p_4 was found to be unnecessary for the present experiments. The data were then recorded and subsequently processed according to procedures outlined above. The value of p_2 computed from Eqn. (2) is known as the dynamic calibration value. The value of p_2 obtained from the output voltage of the transducer and the static calibration, Eqn. (8), is known as the static calibration value.

Results & Discussion

Noise Characteristics

A sample of the unfiltered time trace from the transducer at room conditions (100.3 kPa and 21 °C or 14.55 psia and 70 °F) is displayed in Fig. 4a. The transducer output signal can be written as:

$$V = \bar{V} + V' \tag{9}$$

where $\bar{V}$ is the mean output and V' is the fluctuating component of the signal. These voltages can then be converted into pressure using Eqn. (8), so that

$$p = \bar{p} + p' \tag{10}$$

The standard deviation of the fluctuations ("noise"), σ, increased slightly from 0.2% to 0.25% of the mean, $\bar{p}$, as temperature increased from 0 °C (32 °F) to 100 °C (212 °F). The noise appeared to be practically Gaussian (Fig. 4b). In this figure, the dotted line represents the normalized Gaussian distribution. In addition, the spectrum (Fig. 4c) showed that the noise was of high frequency exhibiting a series of peaks. For determining the effective bandwidth of the transducer, the most significant peak was at 50 kHz, the transducer's resonant frequency. Higher frequency peaks were probably the result of transverse and longitudinal waves in the cavity behind the transducer's diaphragm [1]. Similar features were seen in the probability distribution and spectrum of the noise from signals acquired at atmospheric pressure but at 0 °C and 100 °C (not shown for brevity).

As the applied pressure decreased (keeping temperature constant), the S/N ratio dropped through a combination of a decrease of $\bar{p}$ and an increase in σ. A

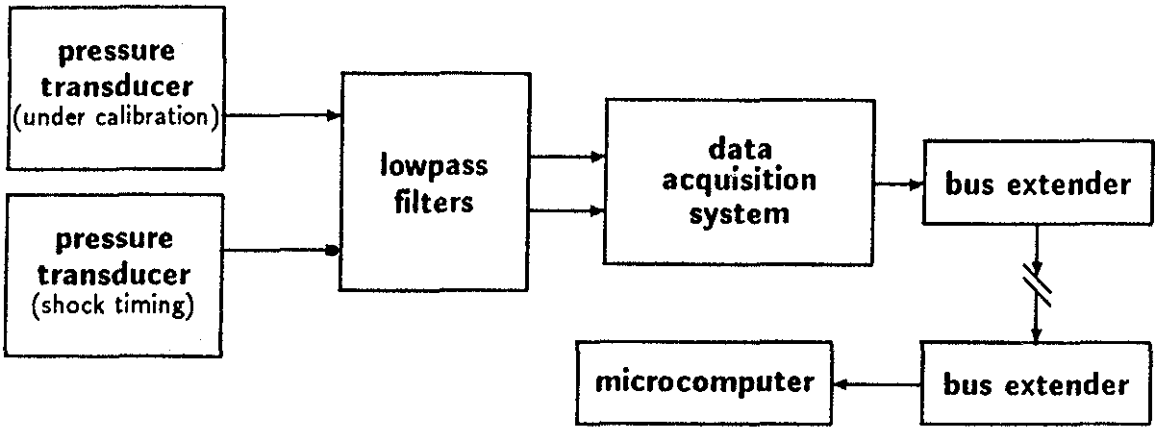

Figure 3: Signal conditioning and data acquisition.

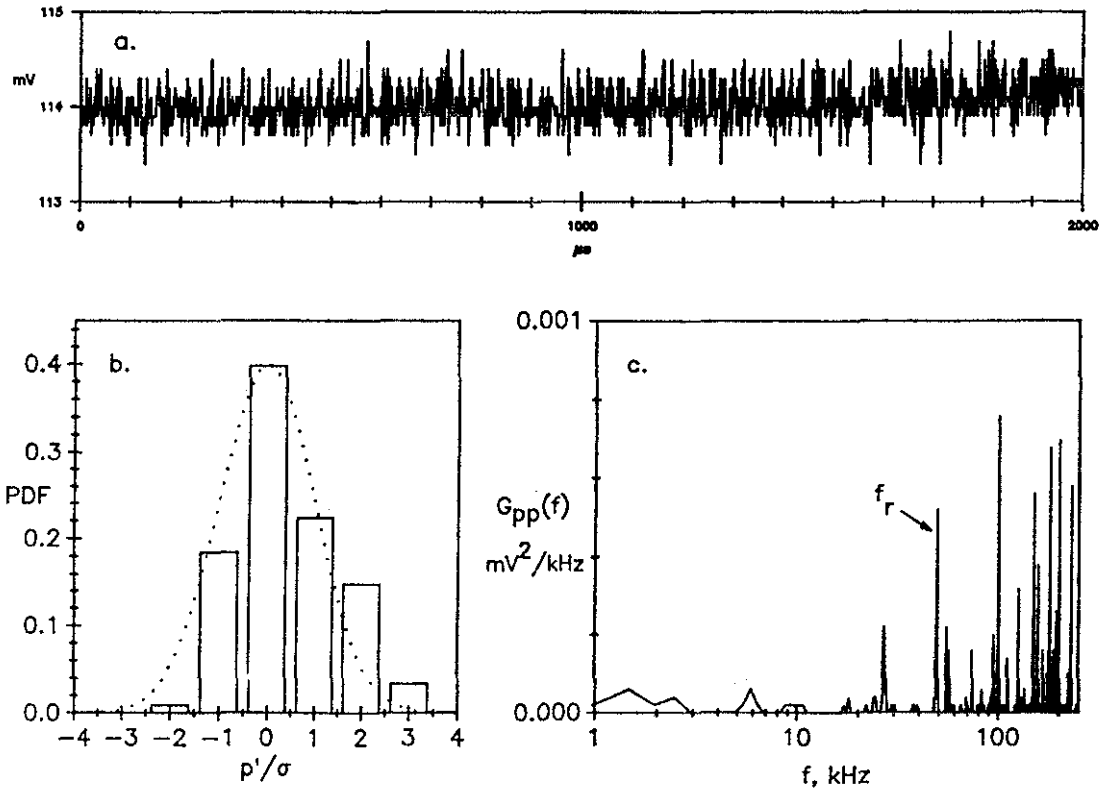

Figure 4: Example of unfiltered record (room conditions). a. Time record. b. Probability distribution. c. Spectrum.

summary plot of the standard deviation data is shown in Fig. 5. Drift data shown in this figure will be discussed subsequently. Thus, at an applied pressure of 1.0 kPa (0.15 psia), the standard deviation of the noise was 0.33 kPa (0.048 psia) or about 30% of the mean. An example of the time record under these conditions is shown in Fig. 6a. This poor S/N ratio emphasizes the importance of filtering the noise from the signal. The probability distribution function of the signal also was Gaussian, Fig. 6b. The spectral peak at 70 kHz, corresponding to transducer resonance, was also seen in the low pressure measurements, Fig. 6c.

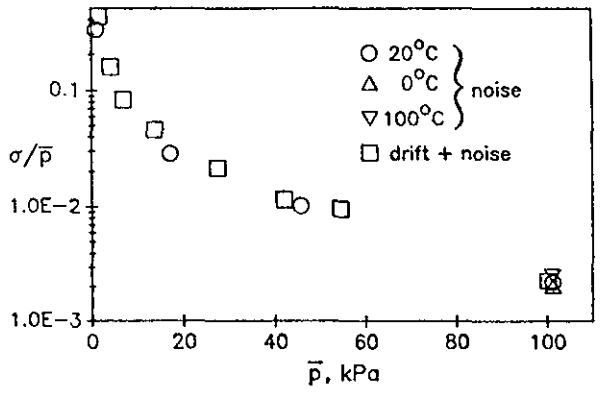

Figure 5: Standard deviation of noise and drift of transducer output.

Drift

Fig. 7a is an example of atmospheric data to illustrate transducer drift. The standard deviation of the signal was about 1% of the mean. This can be compared with the standard deviation of pure noise of 0.2% reported above. The S/N ratio becomes increasingly worse as the pressure decreases. E.g., at 1.69 kPa (0.245 psia), $\sigma \approx 0.43\bar{p}$. This trend is summarized in Fig. 5.

Fig. 7a shows that the signal consisted of small amplitude high-frequency fluctuations (noise) superimposed on the low-frequency drift. The spectrum of the data record (Fig. 7b) showed the 60 Hz AC-line frequency and two peaks at 0.4 Hz and 2 Hz that characterized the drift. Drift causes difficulties since high-pass filtering inevitably also removes the mean. In analyzing pressure signals found in shock boundary-layer interactions using the variable-interval time-averaging (VITA) technique, elaborate procedures are, therefore, necessary to prevent drift from adversely affecting data reduction [1].

Static & Dynamic Calibration

A linear least-squares curvefit of the static calibration data (Fig. 8) gave a sensitivity of

$$c = 1.19\ \mu\text{V/Pa}. \qquad (11)$$

This was about 2.5% below the manufacturer's quoted value. The figure also shows dynamic calibration data which will be discussed next.

An example of a time record showing the shock and expansion wave passage is displayed in Fig. 9. From the data, the output voltage can be directly measured and, using Eqns. (8) and (11), the static calibration pressure was evaluated. The experiments showed that test times were about 1 ms for all the runs. Therefore, a visual inspection of the trace isolated a smaller time segment (0.5 ms giving 250 datapoints) for obtaining the mean output voltage used in evaluating the static calibration pressure. The dynamic calibration pressure was obtained by substituting p_1, M_s and γ_1 into Eqn. (2).

The sensitivity of the transducer obtained from dynamic calibration was found to be $c_{dyn} = 1.21\,\mu$V/Pa, which was 1.6% larger than the static calibration sensitivity. This implies that for a given transducer output voltage, the dynamically determined pressure would be lower than the statically determined pressure, as is shown in the inset to Fig. 8. This result is *different* from Raman's [5]. The discrepancy between static and dynamic measurements may be due to errors in evaluating M_s from measurements of Δt and to transducer drift. The difference may also depend on other factors, e.g., temperature rise due to shock passage. However, no further efforts were made to establish the effects of temperature beside the thermal noise measurements reported above. Essentially, the small error in using static calibration data appears acceptable in dynamic measurements, this error being within the tolerance of conventional fluid-mechanics measurements of pressure. Further, in dynamic measurements of pressure, other instrumentation limitations, e.g., high-frequency noise, bandwidth and spatial resolution, may be even more important in contributing to the accuracy.

Conclusions & Recommendations

Dynamic calibration of a miniature fast-response piezoresistive pressure transducer revealed that mean pressures are below those obtained statically, in contrast to Raman's [5] results. Thus, based on the present experiments, the practice of using statically-calibrated pressure transducers to measure pressure fluctuations would give mean values above actual ones. The noise spectrum revealed that the noise is predominantly above the transducer's resonant frequency. For the temperature range examined, the effect of temperature on transducer noise is negligible. A practical outcome of examining the noise spectrum is that the trans-

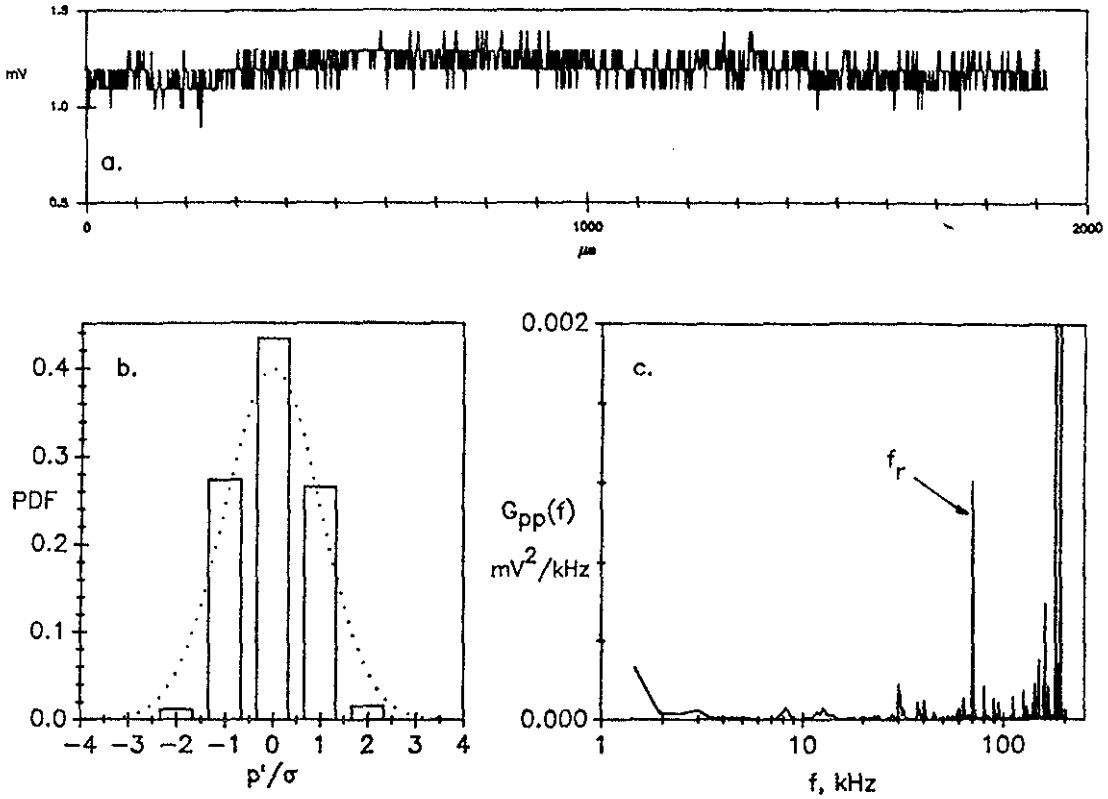

Figure 6: Example of unfiltered record (1.0 kPa and 21 °C). a. Time record. b. Probability distribution. c. Spectrum.

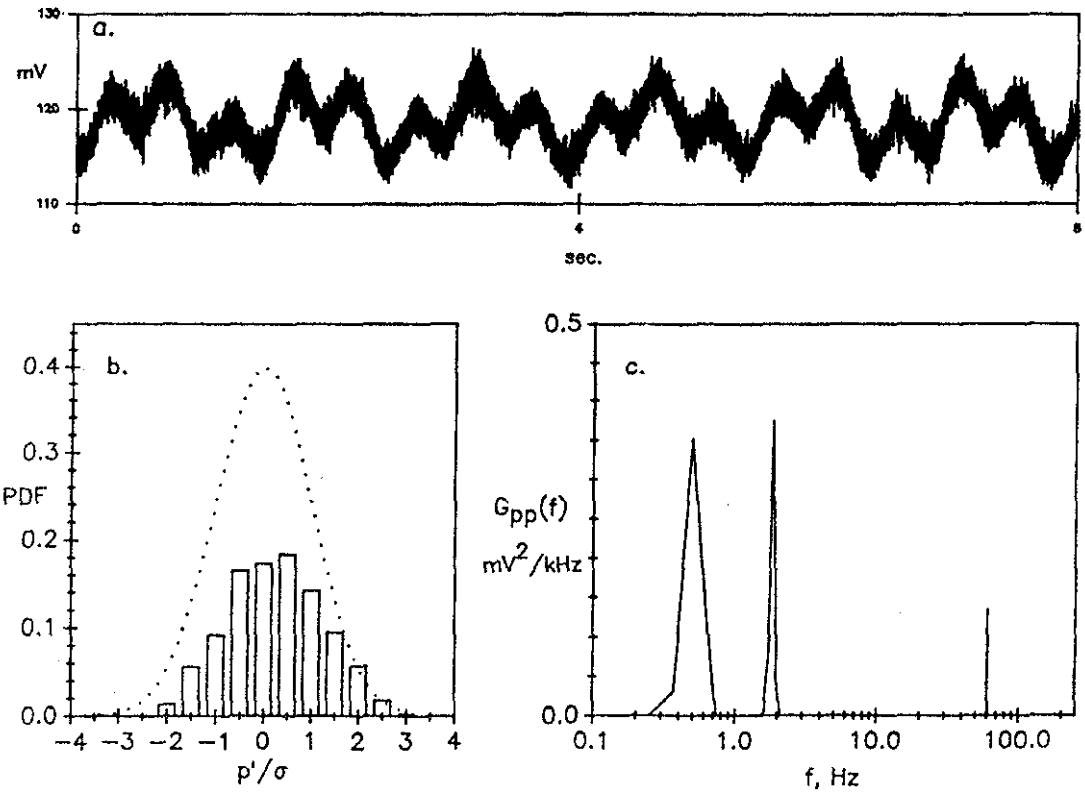

Figure 7: Example of drift in transducer output (room conditions). a. Time record. b. Probability distribution. c. Spectrum.

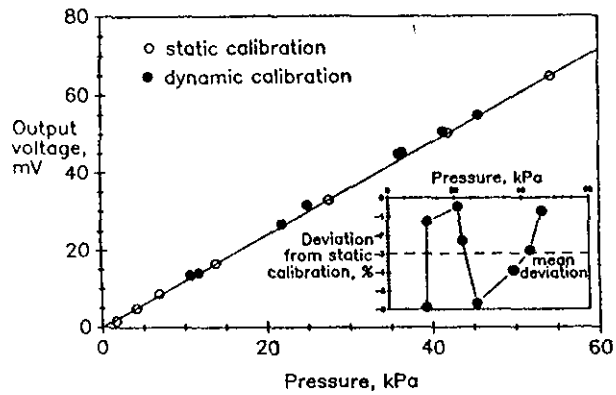

Figure 8: Static and dynamic calibration.

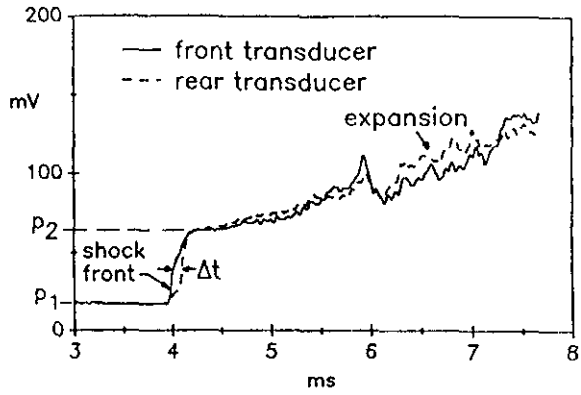

Figure 9: Transducer records of shock and expansion wave passage.

ducer's resonant frequency can be readily determined. Lowpass filtering to improve the S/N ratio is particularly necessary when using the transducers at their low range because of the extremely poor S/N ratio otherwise. Transducer drift decreases the accuracy of mean measurements. Highpass filtering to remove the drift is a viable solution if only pressure fluctuations and not mean values are of interest.

Acknowledgements

The present study was supported by Grant NAG 1-891 from NASA Langley Research Center and monitored by Dr. J. Weidner. The authors thank Jim Holland, ARC technician, and Scott Stuessy for building the test model and for assisting in the experiments. The authors also thank the Dean of Engineering for funding the purchase of the data-acquisition system and the Chairman of the Aerospace Engineering Department for funding the purchase of the host computer.

References

[1] Dolling, D. S. and Dussauge, J. P., "Fluctuating Wall Pressure Measurements," Ch. 8 of *A Survey of Measurements and Measuring Techniques in Rapidly Distorted Compressible Turbulent Boundary Layers*, ed. by H. H. Fernholz, A. J. Smits and J. P. Dussauge, AGARDograph 315, 1988.

[2] Andreopoulos, J. and Muck, K. C., "Some New Aspects of the Shock-Wave/Boundary-Layer Interaction in Compression-Ramp Flows," *J. Fluid Mech.*, Vol. 180, 1987, pp. 405-428.

[3] Tran, T. T. and Bogdonoff, S. M., "A Study of Unsteadiness of Shock Wave/Turbulent Boundary Layer Interactions from Fluctuating Wall Pressure Measurements," AIAA Paper 87-0552, 1987.

[4] Dolling, D. S. and Smith, D. R., "Separation Shock Dynamics in Mach 5 Turbulent Interactions Induced by Cylinders," *AIAA J.*, Vol. 27, 1989, pp. 1698-1706.

[5] Raman, K. R., "Surface Pressure Fluctuations in Hypersonic Turbulent Boundary Layers," NASA CR-2386, 1974.

[6] Soloukhin, R. I., Curtis, C. W. and Emrich, R. J., "Measurement of Pressure," Ch. 5 in *Fluid Dynamics*, Vol. 18, Pt. B., ed. by R. J. Emrich, Academic, New York, 1981.

[7] Bynum, D. S., Ledford, R. L. and Smotherman, W. E., "Wind Tunnel Pressure Measuring Techniques," AGARDograph 145, 1970.

[8] Schweep, J. L., Eichberger, L. C., Muster, D. F. and Michaels, E. L., "Methods for the Dynamic Calibration of Pressure Transducers," NBS Mono. No. 67, 1963.

[9] Bendat, J. S. and Piersol, A. G., *Random Data: Analysis and Measurement Procedures*, 2nd ed., Wiley-Interscience, New York, 1986.

[10] Anderson, J. D., Jr., *Modern Compressible Flow*, 2nd ed., McGraw-Hill, New York, 1982.

[11] Sullivan, J. J., "Development of Variable Capacitance Pressure Transducers for Vacuum Applications," *J. Vac. Sci. Tech. A*, Vol. 3, 1985, pp. 1721-1730.

[12] Alpher, R. A. and White, D. R., "Flow in Shock Tubes with Area Change at the Diaphragm Section," *J. Fluid Mech.*, Vol. 3, 1958, pp. 457-470.

[13] Stuessy, W. S., Murtugudde, R. G., Lu, F. K. and Wilson, D. R., "Development of the UTA Hypersonic Shock Tunnel," AIAA Paper 90-0080, 1990.

[14] Chung, K.-M., "Shock-Tube Calibration of a Fast-Response Pressure Transducer," M.S.A.E. Thesis, The Univ. of Texas at Arlington, 1989.